A New Axial Flux Surface Mounted Permanent Magnet Machine Capable of Field Control

Metin Aydin[1], *Student Member, IEEE* maydin@ieee.org
Surong Huang [2], *Member, IEEE* srhuang@yc.shu.edu.cn
Thomas A. Lipo[1], *Fellow, IEEE* lipo@engr.wisc.edu

[1]Electrical and Computer Engineering Department
University of Wisconsin-Madison
1415 Engineering Drive
Madison, WI 53706-1691, U.S.A

[2]Department of Automation
Shanghai University
149 Yan-Chang Road
Shanghai, 200072, P.R. CHINA

***Abstract* – This paper presents a new axial flux surface mounted permanent magnet (PM) field controlled TORUS type (FCT) machine. Machine structure and principles are explored and the field weakening feature of the topology as well as the advantages of the machine are presented in the first part. The second section introduces the linear model and sizing analysis using generalized sizing equations. Optimization of the machine pole number and power density maximization for the optimum pole number is also achieved. In the third section, 3D Finite Element Analyses (FEA) of the topology are illustrated for different field currents in order to accomplish the machine design and to determine the sizing of the optimum field winding. Furthermore, torque analysis of the FCT machine using 3D finite element analysis is also carried out and illustrated in the paper.**

Keywords* – *Axial flux machines, surface mounted PM machines, TORUS, field control, field weakening, finite element analysis.

I. INTRODUCTION

Axial flux surface mounted permanent magnet machines have been used increasingly in the last decade with the use of high energy magnets for various applications [1-3]. They have several unique features such as high efficiency, high power and torque densities, low rotor losses and small magnetic thickness.

These machines have N stators and N+1 rotors (N ≥ 1) for external rotor and internal stator surface magnet PM disc motor (TORUS) types and N+1 stators and N rotors (N ≥ 1) for internal rotor and external stator surface magnet PM disc motor (AFIR) types. If N is chosen as 1 for external rotor and internal stator structure, the minimum TORUS machine structure can be derived. This machine could be either slotted or non-slotted depending on the stator structure. Slotted TORUS or double-rotor-single-stator type PM machines have been studied in the literature in the past [2-6]. Two different slotted TORUS type machines, namely TORUS NN (North-North) type and TORUS NS (North-South) type, can be derived depending on the direction of the main flux, which are both illustrated in Fig. 1. Both machines have a single stator and two surface mounted PM rotor discs. The stator has a slotted structure with tape wound stator iron. Back-to-back connected windings are placed into back-to-back slots in NN type structure while the conventional 3-phase windings are used in each side of the NS type structure. The rotor structures are exactly the same in both machines, which are composed of surface mounted axially magnetized magnets and rotor discs. The differences between the two structures are the magnetization direction of the magnets, existence of the stator core, the flux paths and winding structure.

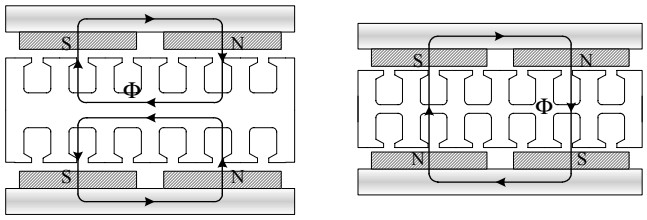

Fig. 1. Structures and 2D flux directions of the NN type TORUS (a) and NS type TORUS (b) machines at the average diameter over two poles

In order to create the appropriate flux path, the magnets facing each other on each rotor should be N and N poles or S and S poles in TORUS NN type and, N and S or S and N poles in TORUS NS type. Therefore, the direction of armature current must be changed appropriately so as to create torque. Since the windings in the radial direction are used for torque production, the end windings of the NN type machine are much shorter than that of NS type machine. In other words, the winding structure used in the NS type machine results in a longer end winding which implies a bigger outer diameter, high copper loss, reduced efficiency and power density compared to its NN counterpart. The fact that TORUS NS type does not require any stator back iron, unlike NN type, since the main flux travels axially gives rise to less iron loss of the NS type machine and implies an increase in power density and efficiency.

Modifying these two TORUS structures by adding one or two DC field windings depending on the machine type to control the airgap flux and providing a path for the DC flux results in two new axial flux double-rotor-single-stator machines with field control capability. The structures of the Field Controlled TORUS NN Type (FCT-NN) and the Field

Surong Huang has been supported by Wisconsin Power Electronics Research Center and National Science Foundation of China (59877014).

Controlled TORUS NS Type (FCT-NS) machines as well as the main flux directions are illustrated in Fig. 2.

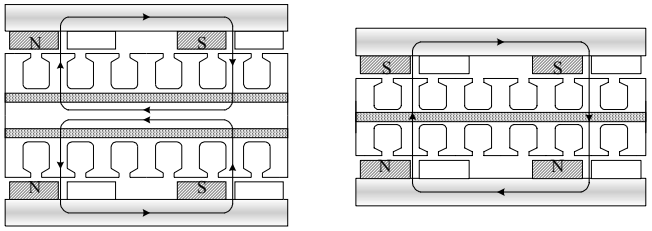

(a) (b)

Fig. 2. Structures and 2D main flux directions of the NN type FCT (a) and NS type FCT (b) machines at the average diameter over two poles

The focus of this paper will be on the FCT-NS type machine. In the first part of this work, the new FCT-NS machine structure and its machine principles are presented. The field weakening feature of the FCT-NS topology as well as the advantages of the machine over its NN counterpart are illustrated. The second section introduces the sizing approach using generalized sizing equations [7-8]. In the third section, optimization of the machine pole number and power density maximization are achieved. A 3D finite element analysis of the topology is illustrated for different field currents in order to prove the machine principle of operation and to determine the sizing of the optimum field winding in the fourth section. Torque analysis of the FCT machine using 3D finite element analysis is also presented in the paper.

II. Flux Weakening of PM Machines

The important limitation of PM machines is the lack of field weakening capability. When we look at electric machines in general, it can be observed that variable speed operation can easily be accomplished by reducing the field current in DC and synchronous machines. However, in PM machines, there exists a fixed magnetic excitation which limits the drive's maximum speed and becomes a significant limitation for both radial and axial flux PM machines. Drives are operated at constant volts per hertz operation up to base speed and constant voltage operation to weaken the field at higher speeds so as to overcome this problem. In order to reduce the field at high speeds, vector control techniques are used. This causes large demagnetization currents in the machine d-axis and increases conduction losses as well. As a large d-axis current is applied, the magnets are made to operate in the irreversible demagnetization region and after the current is removed they may not be able to go back to their original operating point. This feature results in reduced torque capacity of the machine and reduced machine efficiency. Moreover, this mode of operation affects the constant power region of the machine since the demagnetizing current of the magnets limits the constant power region.

It has been of great interest to achieve field weakening in PM machines by eliminating the effects of d-axis current injection. New machine topologies gain importance at this point. There exist some alternative solutions to eliminate this problem in PM machines. New topologies have been introduced in the literature with field weakening from a machine perspective. [9-13]. However, no axial flux machine exists with true field weakening capability in the literature. The new field controlled axial flux surface mounted permanent magnet TORUS type (FCT) machine has been proposed not only to overcome this drawback but also to improve the features of PM machines by introducing a new axial flux structure with flux weakening capability.

III. A New Axial Flux PM Machine Concept With Airgap Flux Control

The field controlled axial flux surface mounted PM machine seen in Fig. 3 has two slotted stator rings realized by tape wound cores with polyphase AC windings, two disc rotors and a DC field winding. The circumferentially wound DC field winding is placed in between the inner and outer stator rings. In theory, there is no need for a stator yoke since the main flux travels from one rotor to the other. However, there has to be enough stator yoke to hold the field winding. The axial thickness of the stator depends on the DC field winding.

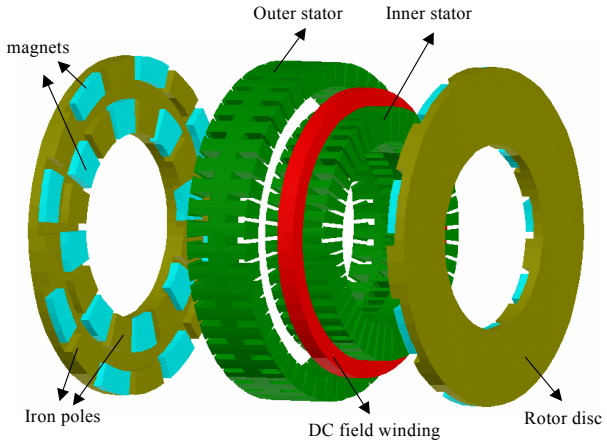

Fig. 3. 3D view of the new axial flux surface mounted field controlled TORUS (FCT) machine

The FCT machine rotor structure is formed by two rotor discs, arc shaped iron pieces, arc shaped surface mounted permanent magnets and a shaft. The two disc shaped rotors carry the axially magnetized NdFeB magnets which are mounted axially on the inner surfaces of the two rotor discs. It should be pointed out that each rotor pole consists of one PM and one iron piece and there exists some space between the magnet and iron piece due to the field winding. The polarity of the magnets on the outer side of the rotor are all the same (say north) and the consequent south poles are formed on the inner sides. In other words, the magnets are positioned such that the north poles are placed on the outer sides and south poles are placed on the inner sides of the rotor disc. Detailed views of the stator and rotor structures of the FCT machine are also given in Fig. 4(a) and 4(b) respectively. The basic flux paths of the FCT machine with no field current are shown in Fig. 5.

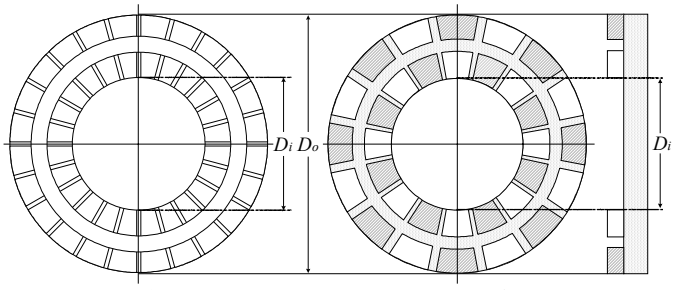

Fig. 4. 2D view of the FCT machine (a) stator and (b) rotor

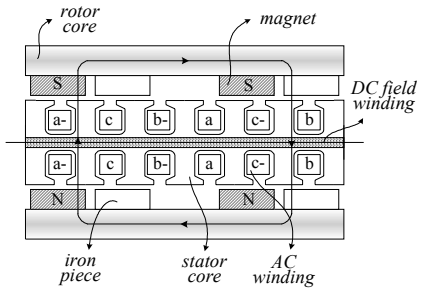

Fig. 5. Main flux directions of the 2 pole portion of FCT machine at the average diameter

IV. Principle of Operation and Airgap Flux Control

There exist two sources of field in the FCT machine, one of which is arising from the permanent magnets and the other arising from the DC field winding. The flux created by the axially magnetized PMs is almost constant and travels from one rotor to the other. This flux is determined not only by the geometry of the magnets but the reluctance of its path as well. As the DC current in one direction (say positive) is supplied to the field winding, the flux created by the field winding travels from one rotor to another through stator, iron piece and two airgaps. The airgap flux can be controlled by this flux component. Depending on the direction of the current the airgap flux can be weakened or strengthened. When both magnet and field sources are combined, the two flux components, one of which is almost constant and the other depending on the level of DC excitation (both direction and magnitude), create variable flux in the machine airgaps.

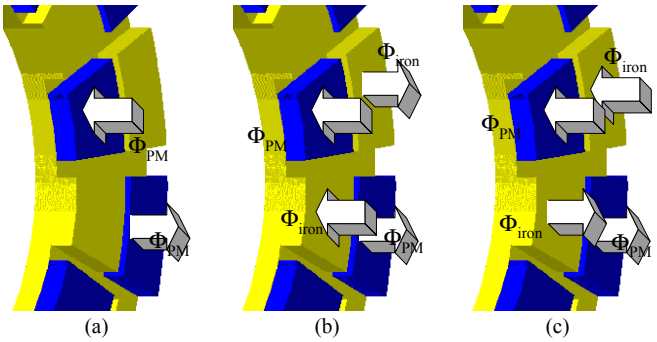

Fig. 6. Airgap flux directions of the FCT machine (a) with no (b) with positive and (c) with negative field currents

Fig. 6 shows the airgap flux directions above the magnet and iron pieces for different field currents and polarities. Fig. 6(a) shows the flux directions with no field current. Fig. 6(b) and 6(c) illustrate the directions of the airgap flux with positive and negative field current cases respectively.

Fig. 7(a) shows the machine flux with no field current. When a positive current is applied to the DC field winding, the average airgap flux is reduced since the flux directions above the magnets and iron pieces are opposite and the DC flux is subtracted from the magnet flux component resulting in reduced airgap flux. As the direction of the field current is changed, the flux direction above the iron pieces changes and the flux created by the field winding is added to the magnet flux. In other words, excitation of the DC field winding of one polarity tends to increase the flux on both inner and outer portions of the rotor pole thus strengthening the magnetic field and increasing the flux linking the stator armature windings. Excitation of the field winding with the opposite polarity will decrease the flux in the consequent poles in both inner and outer portions of the rotor disc thereby achieving field weakening. These two cases are displayed in Fig. 7(b) and 7(c).

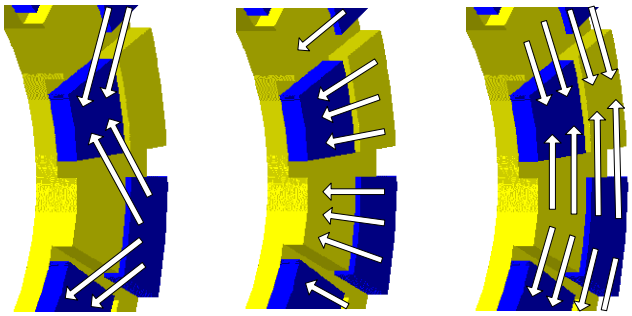

Fig. 7. Flux distribution of the FCT machine (a) with no (b) with positive and (c) with negative field currents

V. Sizing Approach for FCT Machine

The approach for the general purpose sizing equation has been provided in [7] and [8]. The sizing equations have the following forms for axial flux machines:

$$P_R = \begin{cases} \dfrac{1}{1+K_\phi}\dfrac{m}{m_1}\dfrac{\pi}{2}K_e K_i K_p K_L \eta B_g A \dfrac{f}{p}(1-\lambda^2)\dfrac{1+\lambda}{2}D_o^2 L_e \\ \dfrac{1}{1+K_\phi}\dfrac{m}{m_1}\dfrac{\pi}{2}K_e K_i K_p \eta B_g A \dfrac{f}{p}(1-\lambda^2)\dfrac{1+\lambda}{2}D_o^3 \end{cases} \quad (1)$$

where P_R is rated output power of the machine, L_e is effective stack length of the machine, D_o, D_g and D_i are machine diameters at outer surface, air-gap surface and inner surface, K_L is the aspect ratio coefficient and λ is the ratio of the machine inner and outer diameters.

Neglecting the saturation and armature effects and using the principle of flux superposition, the airgap resultant flux can be decomposed into the excitation field of the PM and the excitation field of the DC field winding. Hence, the linear model of the airgap resultant excitation field can be defined as

$$\phi_p = \phi_{p/PM} + \phi_{p/DC} \tag{2}$$

where ϕ_p is the resultant airgap flux over one pole, $\phi_{p/PM}$ is the airgap flux component created by the magnets, $\phi_{p/DC}$ is the airgap flux component created by the DC field winding. They can be written as

$$\phi_{p/PM} = \phi_{PM/PM} + \phi_{iron/PM} \tag{3}$$

$$\phi_{p/DC} = \phi_{PM/DC} + \phi_{iron/DC} \tag{4}$$

where $\phi_{PM/PM}$, $\phi_{iron/PM}$, $\phi_{PM/DC}$ and $\phi_{iron/DC}$ are airgap flux components created by the PM in front of the PM piece, PM in front of the iron piece, DC winding in front of the PM piece and DC winding in front of the iron piece respectively.

Flux values created by PM and DC field windings in front of the PM and iron pieces are

$$\left.\begin{aligned}\phi_{PM/PM} &= B_{g-PM/PM}\ \alpha_{PM/PM}\ S_{PM}\\ \phi_{iron/PM} &= B_{g-iron/PM}\ \alpha_{iron/PM}\ S_{iron}\end{aligned}\right\} \tag{5}$$

$$\left.\begin{aligned}\phi_{PM/DC} &= B_{g-PM/DC}\ \alpha_{PM/DC}\ S_{PM}\\ \phi_{iron/DC} &= B_{g-iron/DC}\ \alpha_{iron/DC}\ S_{iron}\end{aligned}\right\} \tag{6}$$

where, B_g values are peak airgap flux density (created by PM or field winding in front of PM or iron pieces), α values are ratio of average airgap flux density to peak airgap flux density (created by PM or field winding in front of PM or iron pieces) and S is the airgap area.

Using the above equations, the linear model of the airgap flux densities becomes

$$\left.\begin{aligned}B_g &= \frac{\alpha_{p/PM}}{\alpha_p} B_{g/PM} + \frac{\alpha_{p/DC}}{\alpha_p} B_{g/DC}\\ B_{g/PM} &= (\alpha_i \frac{\alpha_{PM/PM}}{\alpha_{p/PM}} B_{g-PM/PM} + \alpha_i \frac{\alpha_{iron/PM}}{\alpha_{p/PM}} B_{g-iron/PM})/2\\ B_{g/DC} &= (\alpha_i \frac{\alpha_{PM/DC}}{\alpha_{p/DC}} B_{g-PM/DC} + \alpha_i \frac{\alpha_{iron/DC}}{\alpha_{p/DC}} B_{g-iron/DC})/2\end{aligned}\right\} \tag{7}$$

where α_p is the ratio of average airgap flux density to peak airgap flux density over one pole and α_i is the pole arc ratio.

In order to make the flux and flux density components clearer, the airgap flux density components created by both magnets and the field winding are illustrated in Fig. 8 for one of the airgaps of the FCT machine. As seen in the figure, $B_{g\_PM/PM}$ and $B_{g\_PM/DC}$ are the airgap flux densities in front of the magnet piece created by the magnet itself and field winding. Likewise, $B_{g\_iron/PM}$ and $B_{g\_iron/DC}$ are the airgap flux densities in front of the iron piece created by the magnet and field winding.

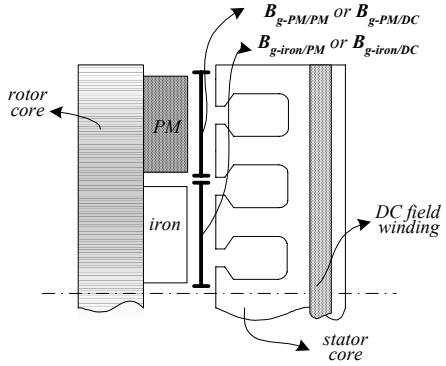

Fig. 8. 2D Illustration of the airgap flux density components of the FCT machine

The component of airgap flux density created by the PM in front of the iron piece can be calculated as

$$B_{g-iron/PM} = -(1 - K_{d-FCTM}) B_{g-PM/PM} \tag{8}$$

where $K_{d\text{-}FCTM}$ is the leakage flux factor between the PM piece and the iron piece, and obtained through a finite element study.

The component of airgap flux density created by the DC field winding in front of the iron piece is derived as

$$B_{g-iron/DC} = K_{fc}\ K_{iron/DC}\ \mu_0 \frac{N_{DC} I_{DC}}{2\, g_e} \tag{9}$$

where N_{DC} is the number of turns of the DC field winding, I_{DC} is the current of the DC field winding, $K_{iron/DC}$ is a correction factor for computation purposes, K_{fc} expresses the field controlled characteristic. It becomes +1 for field strengthened case, 0 for no field current case and –1 for field weakened case.

The component of airgap flux density created by the DC field winding in front of the PM piece becomes

$$B_{g-PM/DC} = -(1 - K_{d-FCTM}) B_{g-iron/DC} \tag{10}$$

From the above equation it is clear that the direction of the component of airgap flux density created by the DC field winding in front of the PM piece $B_{g\text{-}PM/DC}$ is opposite to the direction of the component of airgap flux density created by the DC field winding in front of the iron piece $B_{g\text{-}iron/DC}$.

Using the above linear model of resultant airgap excitation field, the generalized sizing equations can be modified and applied to the FCT machine.

The outer surface diameter of the machine using Equation (1) is

$$D_o = (P_R / \frac{1}{1 + K_\phi} \frac{m}{m_1} \frac{\pi}{2} K_e K_i K_p \eta B_g A \frac{f}{p} (1 - \lambda^2) \frac{1 + \lambda}{2})^{1/3} \tag{11}$$

and the machine total outer diameter D_{tot} for the FCT machines is given by

$$D_{tot} = D_o + 2W_{cu} \tag{12}$$

where W_{cu} is the protrusion of the end winding from the iron stack in the radial direction and can be calculated as

$$W_{cu} = \frac{(0.46 \sim 0.62)D_o}{p}. \tag{13}$$

The axial length of the machine L_e is

$$L_e = L_s + 2L_r + 2g \tag{14}$$

where L_s is axial length of the stator, L_r is axial length of the rotor and g is the axial airgap length. The axial lengths of the stator L_s for both structures are

$$L_s = 2L_{ss-AC} + L_{ss-DC} \tag{15}$$

where $L_{ss\text{-}AC}$ is the axial length of the stator slot for the AC winding, $L_{ss\text{-}DC}$ is the axial length of the stator slot for the DC winding. The axial length of the stator core L_{cs} can be written as

$$L_{cs} = K_{Lcs} \frac{B_g \ \alpha_p \pi D_o (1+\lambda)}{B_{cs} 4p} \tag{16}$$

where B_{cs} is the flux density in the stator core. K_{Lcs} is the correction factor of the axial length of the stator core due to the existence of stator teeth and the DC winding slot. It provides the back path of some flux and hence the axial length of the stator has to be reduced or corrected. The correction factor of the axial length of the stator core K_{Lcs} is relative to the size and shape of the stator slot of the DC winding.

The axial length of the stator slot of AC winding $L_{ss\text{-}AC}$ has to match the axial protrusions of the AC winding. The axial length of the stator slot of DC winding $L_{ss\text{-}DC}$ is derived as

$$L_{ss-DC} = \frac{N_{DC} \ I_{DC}}{H_{ss-DC} \ J_{s-DC} \ K_{cu-DC}} \tag{17}$$

where $H_{ss\text{-}DC}$ the radial height of the stator slot for the DC winding, $J_{s\text{-}DC}$ is the current density of the DC winding and $K_{cu\text{-}DC}$ is the slot fill factor of the DC winding.

The radial height of the stator slot for the DC winding is given by

$$H_{ss-DC} = \frac{D_o - D_i}{K_{ss-DC}} \tag{18}$$

where $K_{ss\text{-}DC}$ is the DC field winding slot factor and can be obtained using FEA.

The axial length of the rotor L_r is

$$L_r = L_{cr} + L_{PM} \tag{19}$$

and the axial length of the disc rotor core L_{cr} is

$$L_{cr} = \frac{K_f \ B_{g-PM/PM} \ \pi D_o \ (1+\lambda)}{K_d \ B_{cr} \ 8p} \tag{20}$$

where B_{cr} is the flux density in the rotor core.

The PM length of the FCT machine L_{PM} can be calculated as

$$L_{PM} = \frac{\mu_r \ B_{g-PM/PM}}{B_r - B_{g-PM/PM} \frac{K_f}{K_d}} (K_{c-AC} \ g) \tag{21}$$

where $K_{c\text{-}AC}$ is the Carter factor for slot effect of the AC winding, $K_{c\text{-}DC}$ is the Carter factor for slot effect of the DC winding and g is the airgap axial length. Both carter factor values can be calculated using FEA.

VI. Optimization of the FCT Machine

A 10 kW, 2000 rpm FCT machine was designed for a specific application. Some optimizations of the FCT machine are accomplished to choose the pole number and meet the space constraints.

A. Optimization of the Pole Number

The key parameters obtained from each design are plotted in Fig. 9 and 10. The plots show the machine efficiency, loss, power density and utilization. It can be seen from the plots that power/torque density values and utilization factors are quite low for lower pole numbers.

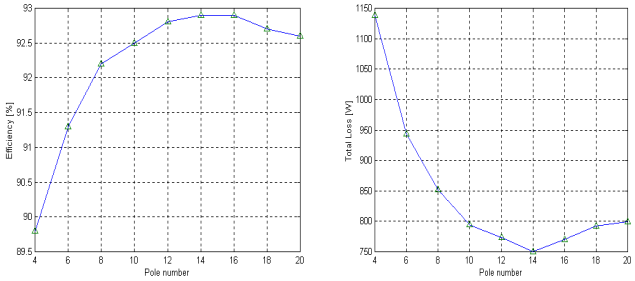

(a) (b)

Fig. 9. Machine efficiency and total loss for different pole numbers

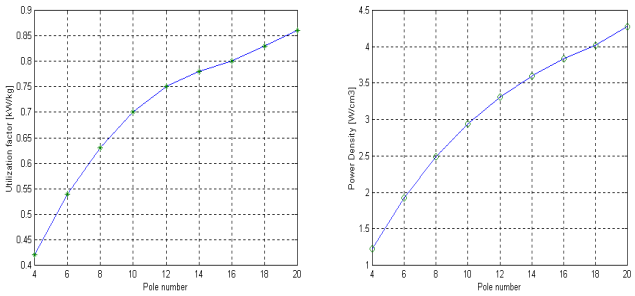

(a) (b)

Fig. 10. Machine utilization and power density for different pole numbers

A reasonable pole number for the new machine after optimization should be 14 or higher because of the radial and axial space limitation of the application and efficiency. If the pole number is chosen to be 16, the machine will not only have the maximum efficiency but also will satisfy the space constraints. In addition, the losses will be closer to the minimum value for that pole number.

B. Optimization of the 16 Pole Machine

Detailed investigation of the 10 kW, 2000 rpm, 16 pole machine is described below. Fig. 11 shows a power density plot of the FCT machine as a function of airgap flux density and diameter ratio with no DC field current. The maximum power density (or torque density) point (MPDP) of the machine can easily be found and the machine can be designed for this point.

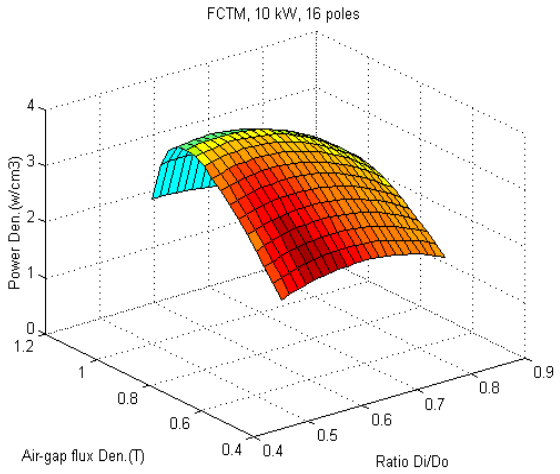

Fig. 11. Power density plot as a function of airgap flux density and diameter ratio (without field winding)

VII. Finite Element Analysis of the FCT Machine

Three dimensional Finite Element Analysis Software, Maxwell© 3D, was used in the analyses. The main purpose of this analyses is realize an overall picture of the saturation levels of the machine, to find the optimum sizing of the field winding, to find out the control range and to investigate the machine torque characteristics.

A. Slot Width Issues for the DC Field Winding

The design of the DC winding slot width is crucial because of the output torque and flux leakage issues. It is important to note that the total effective airgap length that the DC flux has to travel must be greater than the total effective airgap that PM flux has to travel as can be seen in Fig. 12. This condition has to be met not only to prevent the flux short circuit created by the DC field winding but also to effectively use (or to maximize the usage of) the DC flux. In order to avoid this situation and let the DC flux travel through the machine airgaps, slot width should be large enough so that the field ampere turns can be used effectively and be small enough so that the machine torque is close to maximum available torque.

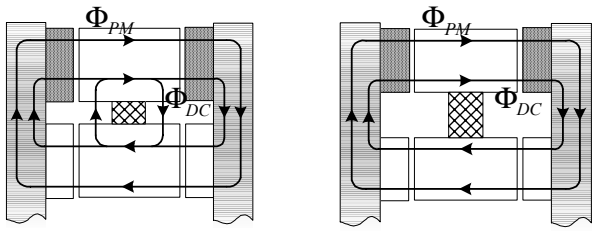

(a) (b)

Fig. 12. PM and DC field flux paths of the FCT machine with (a) small slot width and (b) large slot width

The control range of the FCT machine for different slot widths are investigated in order to find the optimum dimensions for the field winding. For this purpose, the field control range of the machine at no load and full load is investigated for different slot widths for the maximum OD available and other dimensions are calculated using the design code as seen in Fig. 13 and Fig. 14. The machine flux for different slot widths and control ranges at no load condition is shown in Fig. 13. The total machine flux for various slot widths and positive, negative and zero field currents is calculated at no load and the maximum control range is found. The plots indicate that the control range at no load becomes wide for a certain slot width range. As observed from the figure, flux leakage becomes significant for small values of slot width and thereby the machine control range decreases. As for the full load condition, the analysis shows that the control range of the machine is maximum for the slot width of 13 mm. The peak torque will obviously decrease as the slot width increases because DC slot area is not used in the energy conversion. The machine torque values for –1200, 0 and +1200Aturn field current cases are also shown in Fig. 14(b).

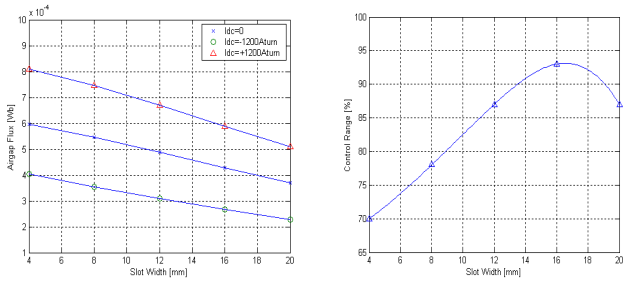

(a) (b)

Fig. 13. Total airgap flux of the FCT machine for different field currents (a) and control range (b) for varying slot width at no load

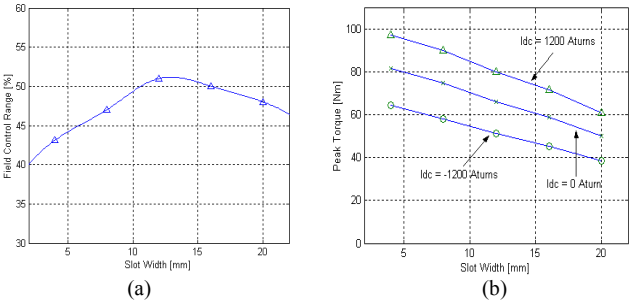

(a) (b)

Fig. 14. Field control range at full load (a) and machine peak torque (b) for different slot width of the DC field winding

B. Finite Element Analysis of the FCT Machine (With Field Winding)

As mentioned earlier, the DC field winding can weaken or strengthen the airgap flux depending on the direction of the field current (I_{DC}). Fig. 15 shows the airgap flux density with flux directions for zero, positive and negative field current cases. As can be seen from the plots the direction of the airgap flux changes depending on the direction of the field current. Since the PM flux does not change with the field current, the total flux in the airgap alters with the field current direction and magnitude. As the field winding is excited, flux directions become either radial or axial depending on the current direction, which represents either weakened or strengthened airgap flux.

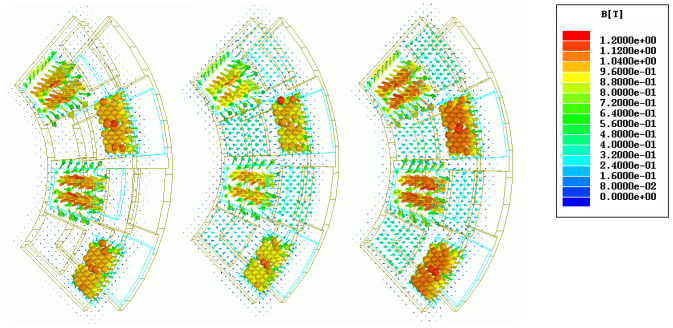

(a) (b) (c)

Fig. 15. Stator and rotor flux density distribution and directions for different values of the DC field current

Fig. 16 illustrates the stator and rotor flux densities as well as the directions of the flux in the rotor for the same field current conditions. Fig. 16(a) shows the flux densities and directions arising only from the magnets since there is no field excitation. As the field winding is excited, seen in Fig. 16(b) and 16(c), the flux directions become either radial or axial depending on the current direction, which represents either weakened or strengthened airgap flux. It should be mentioned that the flux directions in the rotor structures are important as a result of the iron loss since 3 dimensional flux travels in the rotor yoke depending on the direction of the field current.

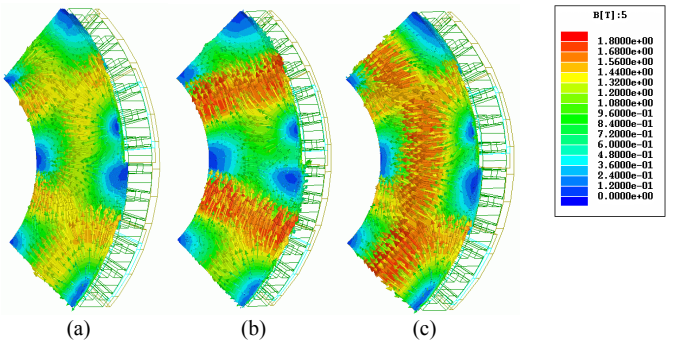

(a) (b) (c)

Fig. 16. Rotor flux density distribution and directions for different values of the DC field current: (a) 0 Aturns, (b) –1200 Aturns, (c) +1200 Aturns current cases

Fig. 17 shows the 3D flux density distribution over one pole for three different cases of the DC field current (0 Aturns, +1200 Aturns and –1200 Aturns). As can be noted from the plots, the flux density magnitude and directions on the iron poles indicate that the flux over one pole can be weakened or strengthened depending on the direction of the DC current. Since the magnet flux does not change with the DC field current, the total airgap flux which is the sum of the PM flux and iron flux alters with the field current direction and magnitude resulting in weakened or strengthened flux in the airgap. The slotting effects of the machine are also evident from the three figures.

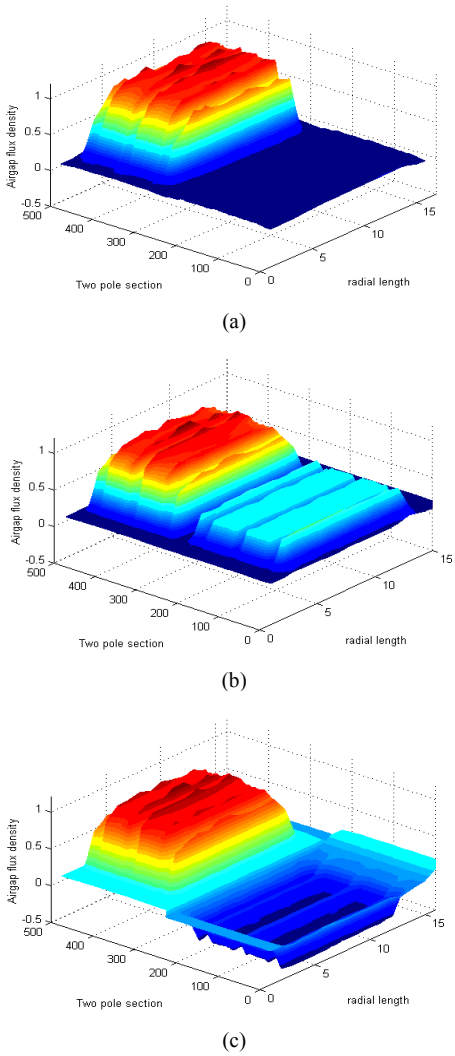

Fig. 17. Airgap flux density distribution of the FCT machine for different values of the DC field current over one pole at (a) 0 Aturns, (b) +1200 Aturns, (c) –1200 Aturns current cases

As mentioned earlier, the airgap flux can be thought of as the combination of magnet flux and iron flux due to DC field winding. Each component of the airgap flux is obtained for different field currents using FEA. The total flux over one pole is also calculated and plotted as the DC field current varies. Fig. 18 shows the airgap flux components including magnet, iron and total flux values over one pole at no load. As can be seen from the figure, the total airgap flux can be weakened or strengthened with respect to the zero DC current case. With the variation of ±1200 Aturns, the airgap flux control range at no load becomes roughly 87%.

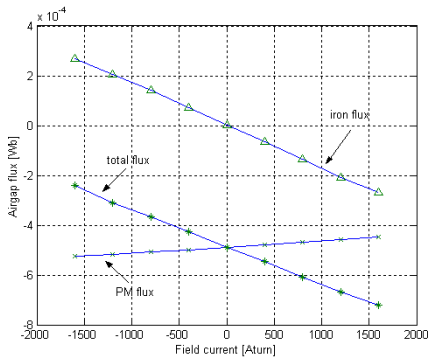

Fig. 18. Airgap flux (PM flux, iron flux and total flux) of the FCT machine over one pole

C. Torque Analysis of the FCT Machine

Analysis of the FCT machine torque is also accomplished. Fig. 19 shows the static torque characteristic of the machine. The plot is obtained for different field current cases over one rotor pole and implies that the machine torque range can be increased by nearly 51% with respect to the zero DC current case.

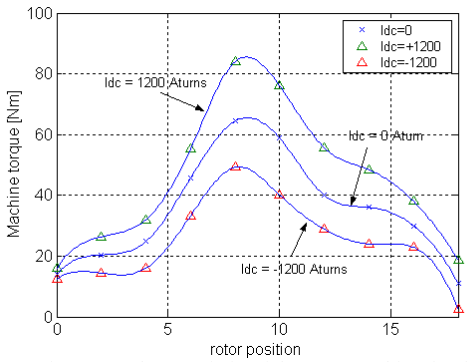

Fig. 19. Static torque characteristic of the FCT machine for different field current values

VIII. CONCLUSIONS

A new axial flux surface mounted permanent magnet field controlled TORUS type (FCT) machine has been presented in this paper. This new FCT machine is the first axial flux surface magnet machine which is capable of true field weakening. First, the machine structure and principles were illustrated. The new NS type FCT machine has significant advantages over its NN counterpart such as reduced iron loss, reduced DC input power, elimination of DC field flux canceled because of opposite field current directions, increased power/torque density and increased efficiency. The field weakening feature of the topology was also presented. The sizing analysis using generalized sizing equations was introduced in the second section. Optimization of the machine pole number and power density maximization for the optimum pole number for a specific application has been accomplished. A 3D finite element analysis of the topology has been illustrated for different field currents not only to accomplish the final machine design but to find an optimum sizing of the DC field winding as well. The machine control range was also investigated using 3D FEA. A reasonable range of field weakening can be obtained with reasonable DC field current. The analyses showed that a nearly 87% control range can be obtained at no load and a 51% control range can be obtained at full load. It was also observed that the control of the FCT machine could be achieved without any demagnetization risk of the magnets because of the airgap flux control. A machine designed with the principles outlined in this paper is under construction and will be the subject of a future paper.

ACKNOWLEDGMENTS

The authors would like to thank Enova Systems for their support of this research presented in this paper.

REFERENCES

[1] P. Campbell, "Principles of a permanent-magnet axial-field DC machine", *Proc. IEE*, Vol. 121, Dec. 1974, pp.1489-1494.

[2] C. C. Jensen, F. Profumo and T. A. Lipo, "A low loss permanent magnet brushless DC motor utilizing tape wound amorphous iron", *IEEE Trans. on Industry Applications*, Vol. 28, No. 3, May/June 1992, pp.646-651.

[3] T. A. Lipo, S Huang and M. Aydin, "Performance assessment of axial flux permanent magnet motors for low noise applications", *Final Report to ONR*, Oct 2000.

[4] S. Huang, M. Aydin and T. A. Lipo, "Low noise and smooth torque permanent magnet propulsion motors: Comparison of non-slotted and slotted radial and axial flux topologies", *IEEE International Aegean Electrical Machine and Power Electronic Conference*, Kusadasi-Turkey, 2001, pp.1-8.

[5] S. Huang, M. Aydin and T. A. Lipo, "TORUS concept machines: pre-prototyping design assessment for two major topologies", *IEEE Industry Applications Society Annual Meeting*, Chicago, 2001.

[6] M. Aydin, S. Huang and T. A. Lipo, "Design and electromagnetic field analysis of non-slotted and slotted TORUS type axial flux surface mounted disc machines", *IEEE International Conference on Electrical Machines and Drives*, Boston, 2001, pp.645-651.

[7] S. Huang, J. Luo, F. Leonardi, and T. A. Lipo, "A general approach to sizing and power density equations for comparison of electrical machines," *IEEE Trans. on Industry Applications*, IA-34, No.1, pp.92-97, 1998.

[8] S. Huang, J. Luo, F. Leonardi and T. A. Lipo, "A comparison of power density for axial flux machines based on the general purpose sizing equation", *IEEE Trans. on Energy Conversion*, Vol.14, No.2 June 1999, pp.185-192.

[9] Y. Li and T. A. Lipo, "A doubly salient permanent magnet motor capable of field weakening", *IEEE Power Electronics Specialists Conference*, 1995; pp.565-571.

[10] B. J. Chalmers, R. Akmese, L. Musaba, "Design and field-weakening performance of permanent-magnet/reluctance motor with two-part rotor", *IEE proceedings*, Vol.145, No.2, March 1998, pp.133-139.

[11] L. Xu, L. Ye, L. Zhen and A. El-Antably, "A new design concept of permanent magnet machine for flux weakening operation", *IEEE Transactions on Industry Applications*, Vol. 31, No. 2, March/April 1995, pp.373-378.

[12] J.A. Tapia, F. Leonardi and T. A. Lipo, "Consequent pole PM machine with field weakening capability", *IEEE International Conference on Electrical Machines and Drives*, Boston, 2001, pp.126-131.

[13] F. Profumo, A. Tenconi, Z. Zhang and A. Cavagnino, "Novel axial flux interior PM synchronous motor with powdered soft magnetic material", *IEEE Industry Applications Society Annual Meeting*, 1998, pp.152-158.